Fingering instability during fracture of a gel block subjected to shear loading

Krishna Kant Kundan[1] and Animangsu Ghatak[1,2,*]

[1]*Department of Chemical Engineering, Indian Institute of Technology Kanpur, Kanpur 208016, India*

[2]*Center for Environmental Science and Engineering, Indian Institute of Technology Kanpur, Kanpur 208016, India*

(Received 29 November 2019; accepted 28 May 2020; published 1 July 2020)

We report here an alternative kind of fingering instability observed during fracture of an unconfined gel consisting of two cuboids joined by a thin gel disk, and all prepared monolithically. When the blocks are sheared across the joint, fracture ensues with the appearance of fingers at the fracture front. The spacing between the fingers remains independent of the shearing speed, planar shape of the joint, and the shear modulus of gel. Importantly this instability appears without any effect of confinement of the gel block, and its wavelength remains dependent on the lateral size of the disk, in contrast to all known instances of fingering phenomena in confined viscous, elastic, and viscoelastic systems.

DOI: 10.1103/PhysRevE.102.013002

I. INTRODUCTION

Soft solids like crosslinked rubbers, elastomers, and gels are used in a variety of engineering, scientific, and biomedical applications, and how such materials would fail when subjected to different kinds of loadings is a subject of much interest. An example is the ubiquitous fingering instability that mediates fracture of such material or their debonding from an adherent when subjected to tensile loadings. When a flexible adherent is lifted off a thin layer of incompressible, elastic, and viscoelastic adhesive bonded to a rigid or flexible substrate, the contact line that separates the adherent plate from the adhesive layer appears wavy with a well-defined wavelength and amplitude [1–5]. A similar instability phenomenon is also observed when a rigid plate is pulled off a layer of adhesive bonded to a rigid substrate; isotropic cavitation patterns appear either at the bulk of the soft solid or at the interface of the adhesive and adherent [6–8]. The former leads to cohesive fracture of the material and the latter leads to interfacial or adhesive failure. The contact line instability and the isotropic instability phenomenon both have been studied extensively in literature [9–13]. These instabilities appear for films with thickness below a critical value as a response to stiff energy penalty associated with the tensile stress that develops in the elastic film [10,14,15]. Here the film is shown to be critically confined, with confinement defined as the ratio of two length scales: thickness of the film, h, and a lateral length scale, q^{-1}. In the context of the contact line instability, this length scale represents the distance from the contact line within which the stresses remain concentrated. For the isotropic instability, the wavelength defines the lateral length scale. The instability patterns appear when confinement, hq, diminishes below a critical value: $(hq)_c < 0.33$; once hq exceeds this threshold limit, the instability disappears.

While in the above examples, the instability occurs at the interface between two solid adherents, a similar instability occurs also at the interface of a soft solid and air. The experiment here involves a layer of ultrasoft elastic gel (shear modulus ∼80–1060 Pa) bonded at its two planar surfaces to two rigid parallel plates; when air is allowed to protrude into the gel, periodically separated "balloon" shaped yet completely reversible fingers appear along the gel-air interface [16–18]. This instability in soft solids looks very much similar to the classical Saffman Taylor instability [19] occurring with liquid inside the confined geometry of the Hele-Shaw cell. The origin of instabilities in liquid and solid systems are however different. Whereas in the former, negative pressure gradient born out of viscous forces is balanced by the surface tension of liquid resulting in the formation of fingers, in the latter, it is the balance of air pressure and elastic stresses coupled with the nonlinear elasticity of the gel that leads to instability. In essence, the general feature of fingering instability in both solid and liquid is found to be the thinness or the confinement of the solid or liquid layer, which becomes evident also from the linear dependence of the separation between fingers on the thickness of the gel layer [1–5,19].

In contrast, we present here another instability for which the requirement of critical confinement no longer remains a necessary condition for the instability to occur, yet the fingering phenomenon very similar to the ones described earlier occurs. The phenomenon occurs during the fracture of a hydrogel block consisting of two cuboidal portions joined by a thin gel disk all prepared monolithically. When one of the cuboids is sheared against the other across the disk joint, fracture propagates beyond a critical shear load, although not in the direction of application of load, but perpendicular to it. The crack line does not remain straight but becomes undulatory with fingerlike structures having well-defined wavelength and amplitude.

II. MATERIALS AND METHOD

Materials. Acrylamide monomer was purchased from Hi-Media and was used as the main monomer. N,N′methylenebisacrylamide and N,N,N′,N′

*Corresponding author: aghatak@iitk.ac.in

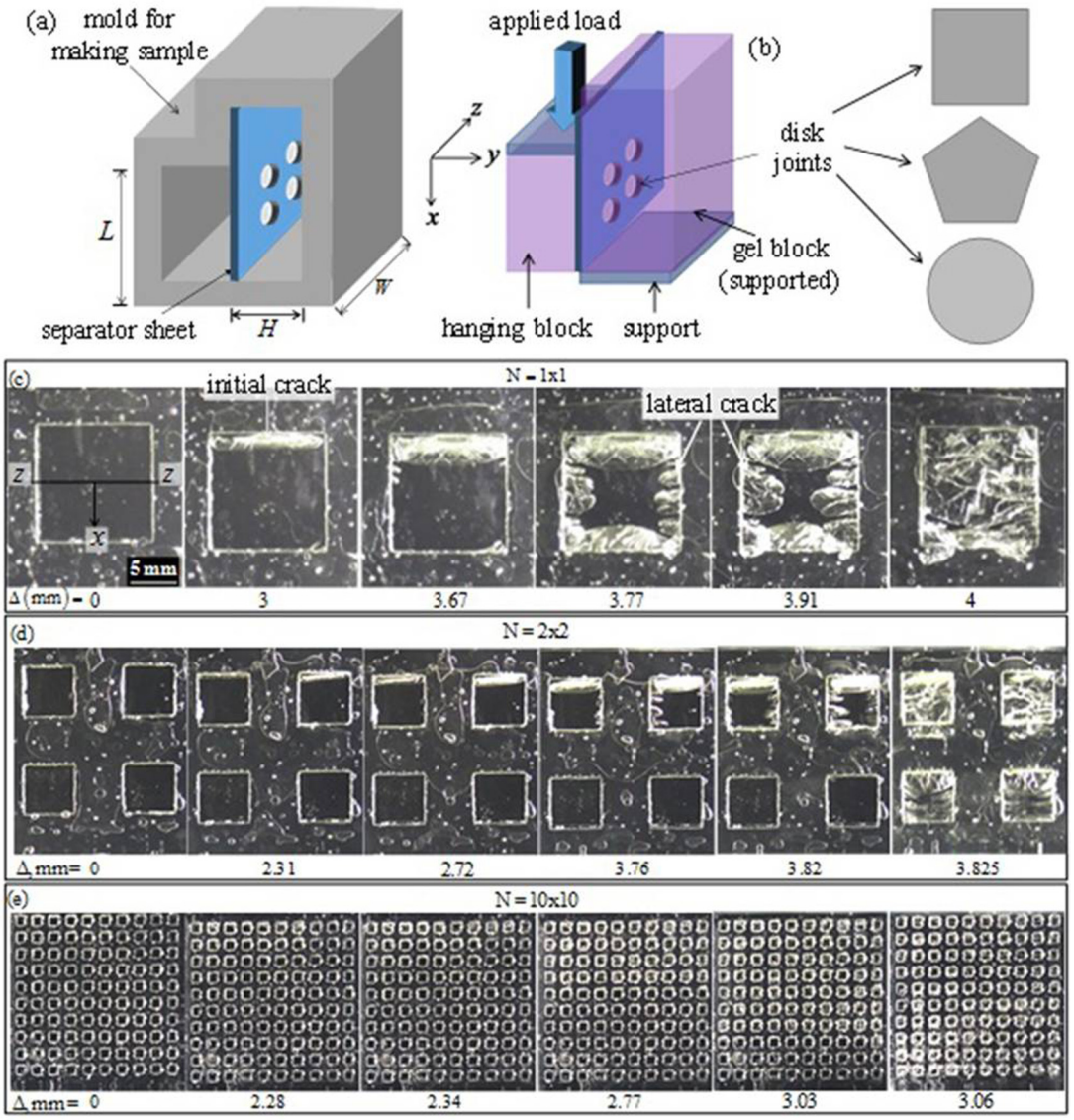

FIG. 1. (a) Schematic depicts the mold in which the gel block was prepared. (b) The schematic of the experiment depicts a monolithic gel block comprised of two rectangular blocks joined by one or more number of tiny gel disks. A portion of the block remains supported on the load cell, whereas the hanging side is loaded vertically down at a controlled rate using a microstage. Gel disks of different shapes are used in experiments. (c)–(e) Sequence of images depicts the progress of fracture for disk joints of different array sizes: 1×1, 2×2, and 10×10. The images are captured at different vertical displacement, Δ, of the hanging side of the block. A gel of modulus $\mu = 40\,\text{kPa}$ is subjected to shear at a constant speed of $V = 31.25\,\mu\text{m/sec}$.

tetramethylenediamine (TEMED) were purchased from Loba Chemicals and were used as the crosslinker and promoter, respectively. Ammonium persulfate (APS) was purchased from Merck and was used as the initiator. These materials were all used as received without further purification. Deionized millipore (DI) water was used for all purposes. Silicone oil of kinematic viscosity 100 cSt was used for lubricating the contact surface between the transparency sheet and the gel.

Method of preparation of gel samples. Hydrogel blocks, each consisting of two cuboidal portions of dimensions $40 \times 28 \times 16\,\text{mm}^3$ and $28 \times 28 \times 16\,\text{mm}^3$ were prepared inside a mold [20], as shown in Figs. 1(a) and 1(b). The gel was prepared by crosslinking an aqueous solution of gel prepolymer solution of acrylamide monomer, N,N′-methylenebisacrylamide (2.67% w/w of monomer), TEMED (4% w/w of monomer), and ammonium per sulfate (0.45% w/w of monomer), all dissolved in deionized millipore (DI) water. The monomer to water ratio was varied in the prepolymer solution, from 35:65 to 10:90, to generate gel having shear modulus 40–7 kPa. The prepolymer solution was crosslinked (for ∼4 min) inside the mold with a thin transparency sheet (thickness ∼50–100 μm) placed at the juncture of the two blocks [20]. An array of holes of different shapes and sizes but of total cross-sectional area $157\,\text{mm}^2$ were drilled into the transparency sheet. After crosslinking, the monolithic gel block consisted of the two cuboidal portions that were connected by gel disks of size and shape as that of the holes in the transparency sheet; this gel desk had the thickness of that of the transparency sheet. The crosslinked gel was

gently removed from the mold, along with the transparency sheet, and was immersed inside a pool of water for 7–10 min to cool it down to ambient temperature. The gel samples, thus prepared, were used in further tests.

Method of carrying out fracture experiments. The gel block consisted of two cuboids: the larger one was fully accommodated inside a housing made of the acrylic sheet, whereas the smaller one was allowed to hang freely under gravity as shown in Fig. 1(b). Vertically downward load was exerted on the hanging portion of the gel along x. Its top surface was pushed vertically down at different rates: 3.75–125 μm/sec using a motorized actuator, thereby exerting a shear load across the gel disk. The load was measured using a load cell interfaced with a computer. The transparency sheet was wetted with silicone oil to minimize the frictional resistance during shearing of the gel [20].

III. RESULTS AND DISCUSSION

The optical micrographs in Figs. 1(c)–1(e) capture the events leading to fracture in a sample which is a square joint. A representative movie of the phenomenon can be seen at the link provided in the Supplemental Material [21]. Here, fracture first initiates towards the top edge of the gel, but soon gets arrested. Instead, lateral secondary cracks emerge almost simultaneously from the two side edges and propagate towards each other along the z direction, i.e., normal to the application of the load. These two cracks eventually coalesce, leading to a complete fracture of the gel block into two pieces. The crack lines do not remain straight, but consist of equally spaced fingerlike protrusions, and propagation of crack essentially occurs via growth of these fingers, which essentially remain pinned at the vicinity of their trough.

Images in Fig. 2 depict typical fracture planes for rectangular and pentagonal single disk joints of different side length, $a = 5 - 20$ mm. Here too fracture was found to occur via appearance and growth of fingers. The morphological evolution of the fingers was examined using high frame rate video photography, which showed that [Figs. 2(i)–2(m)] this instability appears via nucleation of small perturbations spanning the lateral width of the joint. These perturbations grow and coalesce, eventually attaining the final form when the fingertip reaches nearly half of the width of the joint. The perturbations were not found to branch out in contrast to similar fingering instability in viscoelastic films [22–24]. The fingers in their final form were found to remain equally spaced with the distance λ between them increasing with the size of the disk joint, a. Furthermore, λ was almost the same for different disk shapes as long as their linear dimension, a(or diameter d for circle), was nearly constant. Experiments were carried out also with 2×2 and higher-order arrays of disk joints, as presented in Fig. 1(c). These results too show that the wavelength of fingers and their length both get smaller with decrease in the width, a, of individual disks. While, for array sizes exceeding 7×7, λ at the fracture plane of individual disks could not be estimated accurately, the data presented in Fig. 2(h) (symbols ○ and □) show that for arrays of disk joints up to size 7×7, λ was found to scale linearly with a: $\lambda = 0.15a$. This fit included the data obtained from experiments carried out using the gel of different modulus: 7–40 kPa, suggesting that λ remains nearly independent of μ. Similarly, experiments carried out with the shearing speed, V, varied over two orders of magnitude from 3.75 to 312.5 μm/sec show that λ remains unaffected by V unlike fingering instability in confined viscous and viscoelastic films [19,22–24] implying purely elastic origin of the instability.

It is worth noting that the planar shapes of the disk joint so far described were all characterized by a single length scale: the length of the sides of the polygons or the diameter of the circle. In order to understand how the wavelength of the instability would vary for planar shapes which are characterized by two or more different length scales, a few more experiments were carried out using samples for which the aspect ratio of the planar shapes of the joining disks was different from 1. Figure 3 shows examples of such shapes that are characterized roughly by two different length scales, p and q. These samples were all prepared using the gel of shear modulus, $\mu = 30$ kPa, and were subjected to fracture tests as presented in Fig. 1(a). Similar to previous cases, here too fracture occurred in two stages, first via propagation of the primary crack and then the secondary lateral crack. The optical images presented here represent an intermediate stage of propagation of the secondary crack, characterized by the protruding fingers. It is worth noting that, for elongated shapes, e.g., for the rectangle [Fig. 3(a)] and the ellipse [Fig. 3(b)], the secondary crack and the fingers from the two sides of the disk did not appear exactly facing each other; but in contrast to shapes with $p/q \sim 1$, they appeared laterally staggered. This observation implies that, for these shapes, the shear deformation was possibly not exactly uniform throughout the cross section of the joint. Nevertheless, the wavelength data for all these disk shapes were found to superimpose on those obtained earlier as shown in Fig. 2(h), when plotted against an effective planar length scale $a \sim \sqrt{pq}$, suggesting inherent nonlinearity in the problem. So for regular geometries for which $p \sim q = a$, the wavelength scaled linearly with it.

Effect of thickness of disk joint. In order to examine if the thickness h of the gel disk also affects the instability, experiments were done using the gel of modulus $\mu = 30$ kPa and disk thickness h varying over $50 - 600\,\mu$m. Results from these experiments (Fig. 4) show that for $h > 450\,\mu$m fracture is primarily mediated by the primary crack that propagates almost whole through the area of the disk in the direction of application of the load. For a smaller value of h, the lateral secondary crack propagates with the appearance of the fingers. For h varying over an order of magnitude, the characteristic gap between the fingers was nearly independent of it. This result implies that although the appearance of the instability depends on the thickness of the gel disk, the morphology of the instability remains independent of it.

Gel fracture experiment in normal mode. Several characteristics of this instability corroborate with that of the fingering phenomenon observed when a flexible adherent is lifted off a confined elastic adhesive bonded to a rigid or flexible substrate [1,4,5,25], although, unlike the latter, the experiment here is essentially in shearing mode, i.e., in K_{II} mode and not in the K_I mode. In order to examine if the fingering instability during fracture of our gel would occur also during K_I, i.e., the normal mode of loading, the experiment, as in Fig. 5(a) was carried out. Here the hanging part of the gel block was

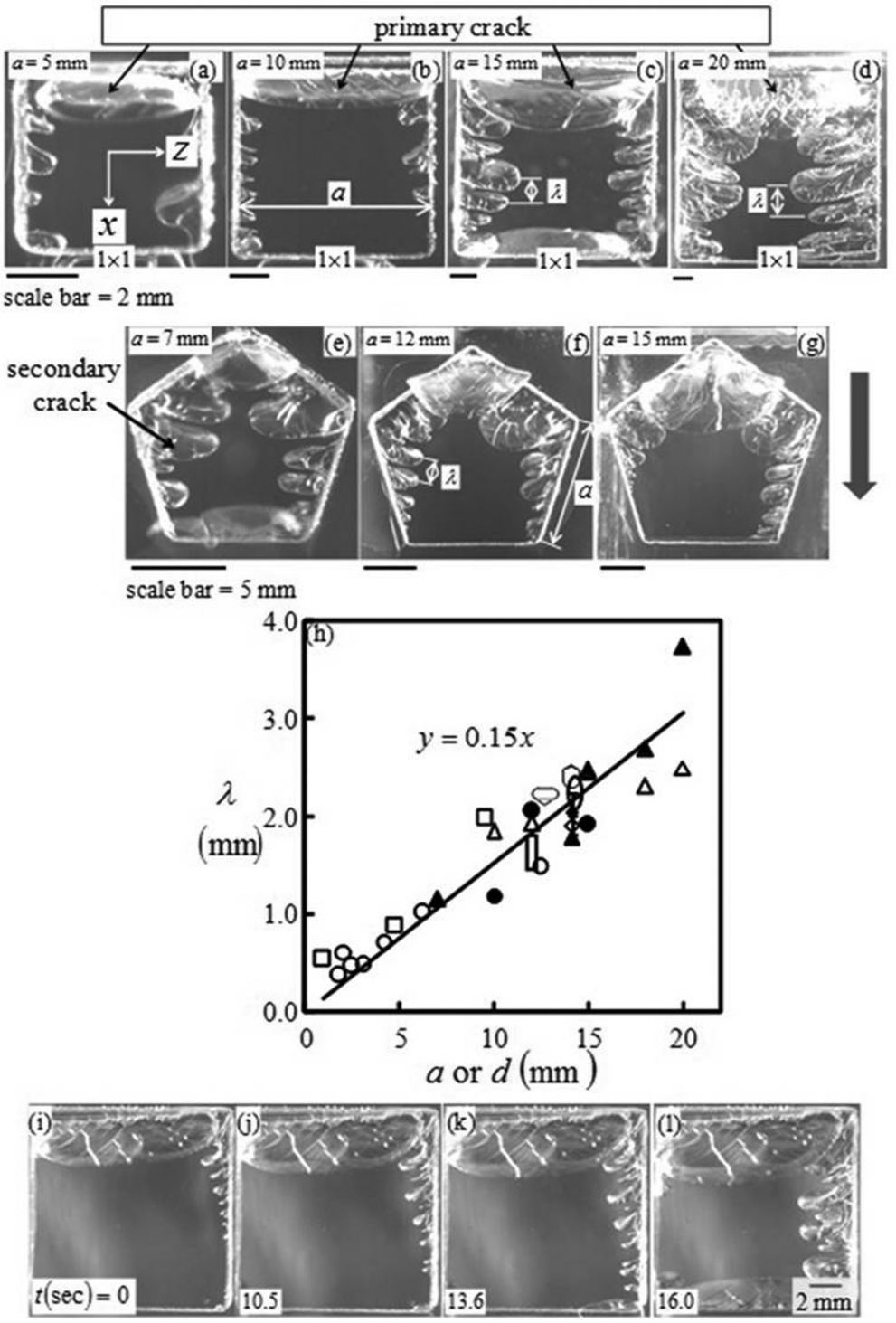

FIG. 2. Images (a)–(d) and (e)–(g) correspond to 1×1 arrays of square joints of size $a = 5 - 20$ mm and pentagonal joint of size: $a = 7 - 15$ mm, respectively. (h) Wavelength λ of instability is plotted against size a of disk joints. Symbols $\circ$ and $\square$ represent arrays of square and pentagon, respectively; the array sizes vary from 1×1 to 10×10. Symbols • represent 1×1 arrays of circular joints of diameters, $d = 10 - 20$ mm. Symbols ▯, ⬯, ⬭, and ⬠ represent disk joints as in Fig. 3. In all these cases, gel blocks of shear modulus $\mu = 30$ kPa are sheared at $V = 31.25\,\mu$m/sec. Symbol ▲ represents 1×1 square array of $\mu = 7$ kPa and $V = 31.25\,\mu$m/sec. Symbol △ represents 1×1 arrays of circles of different d, but of $\mu = 30$ kPa. Symbols ♦ and ◊ represent 1×1 array of circles of $d = 14.14$ mm and $\mu = 30$ kPa and 40 kPa, respectively. These joints were sheared at speed varying from $V = 3.75$ to $312.5\,\mu$m/sec; the error bars represent the standard deviation in λ values. The solid line represents the best fit of the data according to the solution of Eq. (4). (i)–(m) Sequence of images captured at different times depicts the evolution of fingers on the crack front when gel with $\mu = 30$ kPa is sheared at $V = 31.25\,\mu$m/sec.

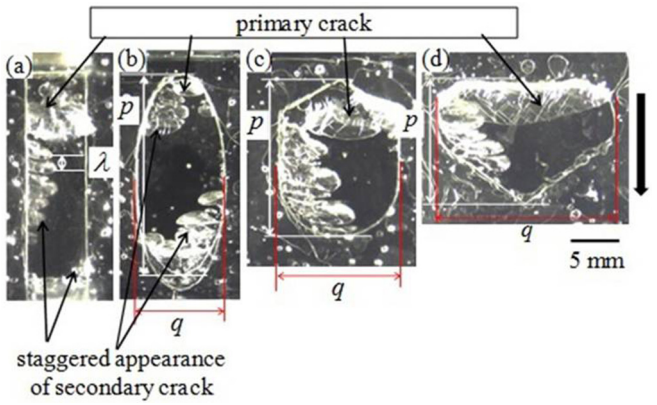

FIG. 3. Experiments were carried out using planar shapes of joints for which the aspect ratio was different from 1. The arrow denotes the direction in which the shear load was applied. The p/q ratio for images (a) to (d) were 4.0, 2.24, 1.36, and 0.68, respectively.

pulled in a displacement controlled experiment off the portion of the gel that remained housed inside the holder. A crack was found to initiate from the loaded side of the disk joint and to propagate whole through its area (as shown by the dashed arrow). However, unlike previous experiments, here the crack front was unwavy and straight [Figs. 5(b)–5(d). Experiments with disks of different shapes showed this behavior suggesting generality of the result. This observation can be rationalized by considering that the thickness of the gel block, measured normal to the plane of the disk joint, $2 \times H = 32$ mm, exceeds the lateral dimension of the gel disk, $d = 12.5$ mm, implying that the gel block is essentially unconfined. For a soft elastomeric layer, which is less than critically confined, the fingering instability does not occur when fractured in the K_I or the lift-off mode. Yet, fingers do appear when the gel block is loaded in the shearing or the K_{II} mode without any apparent confinement of the gel.

Fingering instability in unconfined systems has been observed earlier with liquid films subjected to body or surface forces, e.g., the free surface of a liquid flowing down an inclined plane under gravity [26–28], a circular liquid disk dispensed on a spinning plate subjected to centrifugal force [29,30], and the surface of a liquid layer subjected to thermal Marangoni stress [31,32]. A similar phenomenon is observed also at the interface of a liquid and a soft solid. For example, Marangoni stresses induced by an aqueous surfactant solution dispensed on the surface of agarose and gelatin gel is found to cause fracture on the gel surface which propagates via protruding fingers [33–35]. The common feature in all these examples is that the fingering instability occurs without any confinement of the film and, therefore, the wavelength of instability is mediated by the surface tension and/or gradient

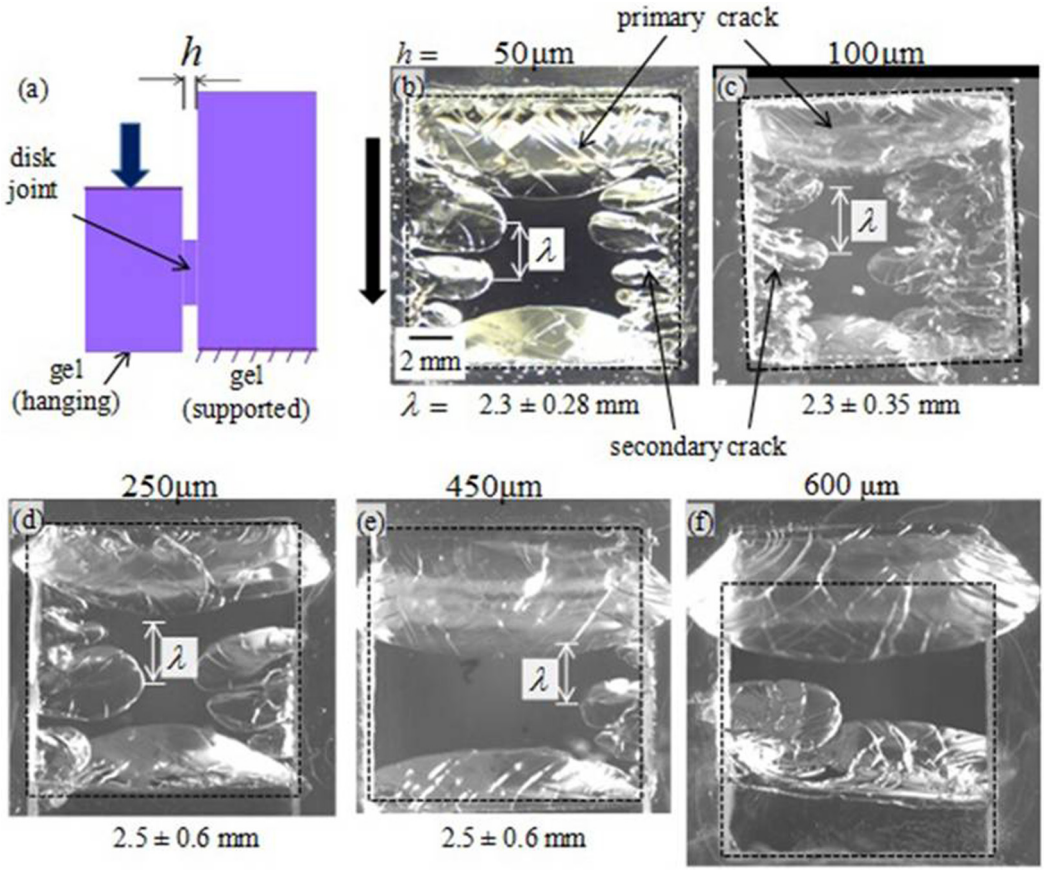

FIG. 4. Thickness, h, of the disk joint (square) was varied and the gel block was subjected to shear loading as in the experiment of Fig. 1. The arrow represents the direction in which the load was applied. Optical images represent the fracture plane at a typical intermediate state of fracture. Gel blocks of shear modulus 30 kPa were used in these experiments. The dotted box in each case represents the boundary of the joint.

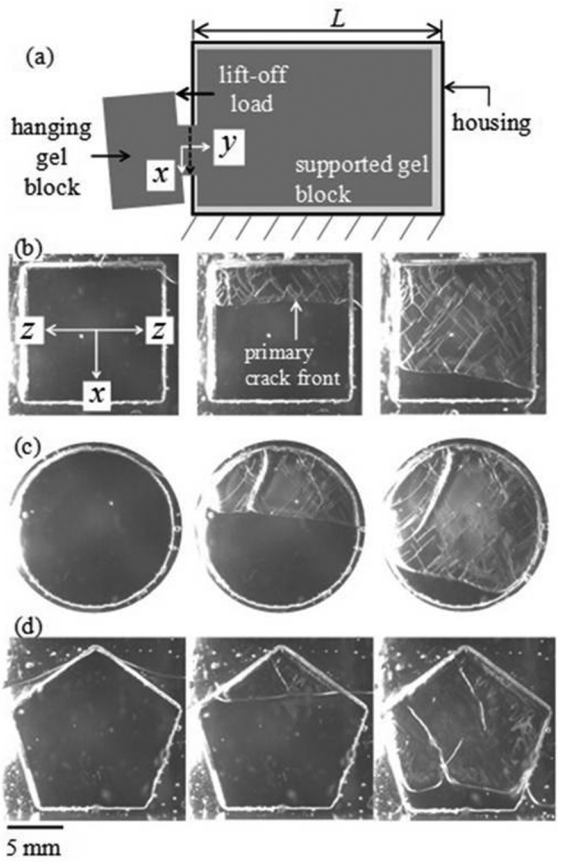

FIG. 5. (a) Schematic shows the experiment in which the hanging portion of the gel block (shear modulus $\mu = 30$ kPa) is peeled off the portion that remains supported inside the housing by application of a lifting load. A motorized manipulator is used to exert the load at a speed of $V = 31.25\,\mu$m/s. The dotted arrow represents the direction in which the crack propagates. (b)–(d) Sequence of images depicts the progress of fracture along the plane of disk joints of three different shapes.

in surface tension of the liquid. For a typical gel used in our experiments, with elastic modulus, $E = 6$ kPa, and surface tension, $\gamma = 60\,\mathrm{mJ/m^2}$, the elastocapillary length can be calculated as $l_c = \gamma/E = 10\,\mu$m, which is an order of magnitude smaller than the wavelength of the instability observed in experiments. This result suggests that the surface tension of the gel does not determine the wavelength of the instability in our experiments.

Analysis of initiation of primary and secondary crack. Initiation of primary and secondary cracks during shear loading of the gel can be understood by considering an ideal situation in which the supported portion of the gel block is subjected to shear deformation along x over the cross-sectional area of the disk joint by the hanging portion of the gel. Figure 6 elaborates the geometry in which the supported gel, represented by an elastic half space, is indented by a flat punch having a square cross section of the size 2α that is representative of the hanging portion of the gel and the disk joint. The elastic half space remains bounded at $y = 0$. Since the shear deformation along x : $u|_{y=0}$ remains uniform along the x and z axes, the distribution of shear stress can be written as [35]

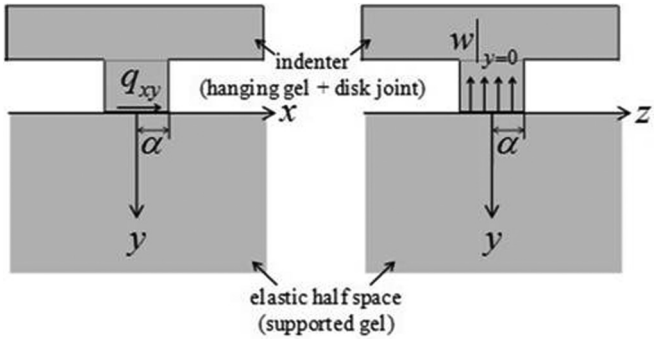

FIG. 6. Side view of indentation of an elastic half space in $x - y$ and $z - y$ plane.

$q_{xy} = q_0(1 - x^2/\alpha^2)^{-1/2}$. The stress distribution results in a singularity at the edge of the area of contact, which in the limit, $x \to \alpha$, can be expressed as $q_{xy} \sim q_0\sqrt{\alpha}/\sqrt{2(\alpha - x)}$. This stress singularity can induce shear fracture as it initially happens from the top edge of the disk joint in our experiments via nucleation of the primary crack. Interestingly, however, the primary crack does not propagate whole through the cross section of the joint but gets arrested possibly because of the coupled effect of crack blunting and a competing secondary crack that emanates from the side of the area of contact. Initiation of the secondary crack from the side of the disk joint can be rationalized by considering that shear loading of the form $q_{xy} = q_0(1 - x^2/\alpha^2)^{-1/2}$ on the surface of the elastic half space leads to a finite displacement along the $-y$ direction, i.e., normal to its surface [36]:

$$w|_{y=0} = -\frac{(1-2\nu)q_0\alpha}{2\mu}\frac{\alpha}{x}\left\{1 - \left(1 - \frac{x^2}{\alpha^2}\right)^{1/2}\right\}. \quad (1)$$

For an incompressible material with the Poisson ratio, $\nu \to 0.5$, the displacement $w|_{y=0}$ vanishes, but for compressible materials with finite compressibility, it remains finite. It has been shown earlier [37] that acrylamide gel is compressible with Poisson ratio varying over, $\nu = 0.45 - 0.47$, which suggests that $w|_{y=0}$ is nonzero in our experiments. The negative value of $w|_{y=0}$ implies that this displacement corresponds to an equivalent pulling stress $\sigma_{yy}|_{y=0}$ on the elastic half space. It is to be noted that equation $w|_{y=0}$ remains uniform along the z axis; drawing an analogy from the indentation of an elastic half space by a rigid flat punch, it can be concluded that the stress field σ_{yy} then varies along the z axis as [36] $\sigma_{yy}|_{y=0} = \sigma_{y0}(x)(1 - z^2/\alpha^2)^{-1/2}$ in which the prefactor $\sigma_{y0}(x)$ can be deduced from Eq. (1) as [36]

$$\sigma_{y0}(x) = \frac{(1-2\nu)q_0}{\pi(1-\nu)}\frac{\alpha}{x}\left\{1 - \left(1 - \frac{x^2}{\alpha^2}\right)^{1/2}\right\}. \quad (2)$$

Since the tensile stress $\sigma_{yy}|_{y=0}$ remains singular at $z \to \alpha$, the secondary lateral crack can indeed nucleate at $z = \pm\alpha$ and can propagate along the z axis as observed in our experiments. In other words, the compressibility of the material can lead to mode I fracture as in a classical peeling or lifting plate experiment although no peeling or lifting load is applied.

In order to rationalize the presence of undulation at this crack front, as shown by the schematic as in Fig. 7, we now

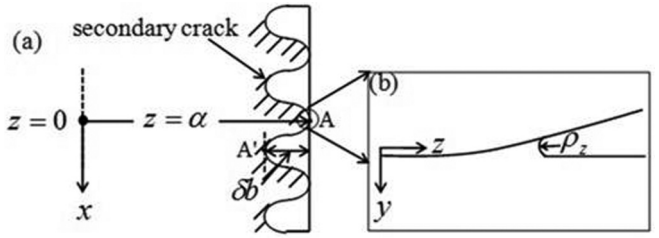

FIG. 7. (a) Schematic of the xz plane shows the occurrence of fingers along the x axis that propagates along z. Points A and A′ define two typical locations along the crack front. δb is the amplitude of the perturbation. (b) The schematic shows a typical yz plane at the vicinity of the crack front.

consider the stress field in the gel at the vicinity of the crack tip. In the limit $z \to \alpha$, this stress field can be expressed as $\sigma_{yy} \sim \sigma_{y0}(x)\ \sqrt{\alpha}/\sqrt{2(\alpha - z)}$. The expression for $\sigma_{yy}|_{z\to\alpha}$ has the general form $\sigma_{yy}|_{z\to\alpha} = K_I/\sqrt{2\pi(\alpha - z)}$ in which the numerator is replaced by the mode I SIF, $K_I = \sigma_{y0}(x)\ \sqrt{\pi\alpha}$. The stress singularity inherent in the above expression implies that for a brittle solid the radius of curvature at the crack tip equates to zero. However, for deformable materials, one expects significant crack blunting, leading to a tip having parabolic shape of finite radius of curvature [14,37–41] ρ_z. The exact nature of ρ_z has been a subject of significant study in the context of fracture of materials of different types: elastic, elastoplastic, and viscoelastic. The summary of these studies is that the crack tip radius is a physical quantity that depends upon both material and geometric parameters. For example, for fracture of an elastoplastic material [41], it depends upon the elastic modulus, E, yield stress of the material, σ_Y, and the fracture energy, Γ:$\rho_z = E\Gamma/\sigma_Y^2$. On the other hand, in the context of peeling a viscoelastic adhesive tape off a rigid substrate, considering that fracture energy depends upon peel angle, θ, ρ_z is expected to vary with the peel angle [39,40] as $\rho_z = P(1 - \cos\theta)/\omega E$, where P is the peeling load and ω is the width of the tape. For lifting a flexible plate off an elastic adhesive material [14], ρ_z can be shown to decrease with an increase in the crack length defined as the distance of the crack front from the line of application of the lifting load. Similar to these solids, for fracture of the soft gel in our experiment too, ρ_z (Fig. 7) is expected to be a function of the crack length, δb: constant for a straight crack ($\delta b = 0$) that spans along the x axis but varying along the contour length of an undulatory crack. While the undulatory contour of the crack front can be expressed as a superposition of several Fourier modes, for simplicity we can consider only the dominant mode of wavelength λ, so that the crack length can be defined as $\delta b = (A/2)[1 + \sin(2\pi x/\lambda)]$; here A is the amplitude of the dominant mode. Drawing analogy from the lifting plate experiment [14], ρ_z can be expected to decrease with the crack length δb, so that it is smaller at point A′ with respect to that at point A. As a first approximation, ρ_z can be expressed as $\rho_z(b) = \rho_{z0}(1 - c\delta b/\alpha)$, where $c > 0$ is a proportionality constant. Since the stress at the crack tip is expressed as [38–40] $\sigma_{yy}|_{\text{crack tip}} = K_I/\sqrt{2\pi\rho_z}$, at location A on the crack front it can be expressed as $\sigma_{yy}|_A = K_I/\sqrt{2\pi\rho_{z0}}$, whereas at A′, it can be expressed as $\sigma_{yy}|_{A'} = K_I/\sqrt{2\pi\rho_{z0}(1 - c\delta b/a)} \sim K_I(1 + c\delta b/2\alpha)/\sqrt{2\pi\rho_{z0}}$. Thus the effective SIF at A′ increases to $K_I^* \sim K_I(1 + c\delta b/2\alpha)$. Using this expression for SIF, the corresponding strain energy release rate can be written as $G_I = (1 - \nu^2)(K_I^*)^2/2E \sim (1 - \nu^2)K_I^2(1 + c\delta b/2\alpha)^2/2E$, where E and ν are respectively the Young's modulus and Poisson ratio of the material. This relation suggests that, for a finite value of δb, the strain energy release rate at A′ remains higher than that at A. Since the velocity of crack propagation increases with the strain energy release rate [42,43], any perturbation at the crack front is expected to amplify with the crest point A′ propagating faster than the through point A on the crack front, implying that the system is inherently unstable so that any undulation at the crack front is expected to grow.

We will now show that, with an increase in the amplitude of the perturbations, their wavelength is also expected to increase. This aspect can be understood by considering that the strain energy release rate calculated over the contour length of the propagating crack front equates to the fracture energy of the material:

$$\frac{1}{\lambda}\int_0^l \frac{(1 - \nu^2)(K_I^*)^2}{2E} dl = G. \tag{3}$$

Here

$$l = \int_0^\lambda \sqrt{1 + (\partial\delta b/\partial x)^2}\, dx$$
$$= \int_0^\lambda \sqrt{1 + (A\pi/\lambda)^2 \cos^2(2\pi x/\lambda)}\, dx$$

is the contour length of the crack front over one wavelength of the perturbation. During crack propagation, SIF attains a critical value, K_I, which remains independent of the lateral location x. The expression for fracture energy can be rewritten as [44]

$$G \sim \frac{(1 - \nu^2)K_I^2}{2E\lambda}\int_0^\lambda \sqrt{1 + \left(\frac{A\pi}{\lambda}\right)^2 \cos^2\left(\frac{2\pi}{\lambda}x\right)}\, dx.$$

The proportionality in the expression of G accounts for the approximations made in defining K_I. In the limit $A \to 0$, i.e., for a straight mode I crack without any undulation, $G \sim (1 - \nu^2)K_I^2/2E$. For fracture of a crosslinked gel, fracture energy, G depends upon the number of bonds broken per unit area and it remains constant irrespective of the undulatory nature of the crack. The expression for wavelength can be written in an implicit form as

$$\lambda = C\int_0^\lambda \sqrt{1 + (A\pi/\lambda)^2 \cos^2(2\pi x/\lambda)}\, dx,$$

where C is the proportionality constant. Furthermore, since the wavelength between the fingers is measured when the length of the fingers reaches nearly half of the width of the joint, the amplitude A can be replaced by α. The expression for wavelength then yields

$$\lambda = C\sqrt{(1 + (\alpha\pi/\lambda)^2)}$$
$$\times \int_0^\lambda \sqrt{1 - [(\alpha\pi/\lambda)^2/(1 + (\alpha\pi/\lambda)^2)]\sin^2(2\pi x/\lambda)}\, dx. \tag{4}$$

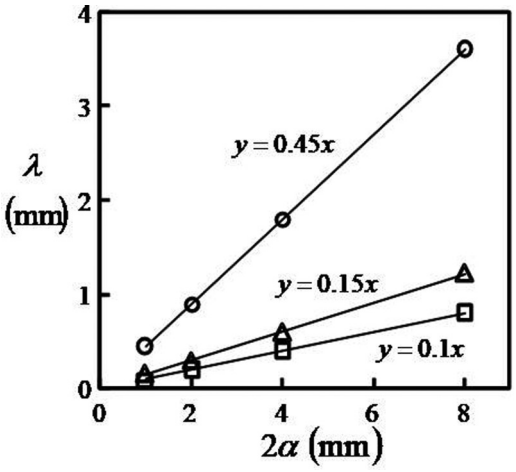

FIG. 8. Equation (4) was solved for different values of prefactor C and α. For a given value of C, the λ vs 2α data were found to fall on a straight line. Symbols ○, △, and □ represent $C = 0.4$, 0.15, and 0.1, respectively.

Note that the integral in the above expression defines the elliptic integral of the second kind which is evaluated numerically to obtain λ for a set of given values of prefactor C and α (Fig. 8). The solid line in the plot of Fig. 2(h) also summarizes the results from these calculations. For a given value of C, the wavelength of the instability λ indeed increases with the spatial dimension of α of the disk joint. For $C = 0.15$ the λ vs α plot best fits the data obtained from experiments. While the above analysis captures the experimental observations and explains the scaling of wavelength, a more rigorous stability analysis of the experiment will be required to capture the dynamic evolution of the waves and to understand what determines the prefactor.

IV. SUMMARY

To summarize, we have presented here a fingering instability that occurs during fracture of a monolithic, multicuboidal gel block when subjected to shearing load. Two portions of the gel are sheared against each other across a disk joint, which results in two undulatory mode I cracks propagating along the plane of the disk in a direction normal to the direction of application of the load. While several features of this instability match closely with other well-known fingering phenomena in confined, incompressible, elastic, and viscoelastic systems subjected to peeling or lifting plate experiments, what distinguishes it from others is that it occurs at the bulk of an unconfined gel block and the wavelength of the instability varies linearly with the lateral dimensions of the plane in which they appear. Importantly, the fingering instability does not appear when the gel block is subjected to conventional peeling load that drives mode I fracture in it. The origin of the instability cannot be attributed to gradient in hydrostatic pressure, which is known to drive fingering phenomenon in a confined liquid system, as the cuboids are subjected to shearing stress across the joining disk. This instability is different also from "bulk elastic instability" in a soft confined gel in which balloon shaped fingers appear even before fracture ensues [16,17]. Unlike these experiments, the gel materials used here are of higher modulus and the instability occurs essentially in an unconfined system. The phenomenon described here is different also from elastocapillary instability mediated by the surface tension of the solid [45]. This difference can be linked to the difference in corresponding elastocapillary length, $l_{EC} \sim \gamma/E$, in these two different systems. Whereas in the previous study [45], $l_{EC} \sim 1.8$ mm, here it was calculated to be 10 μm or less, which is significantly smaller than all dimensions of the gel and also the wavelength of the instability. Our analysis shows that it is the finite compressibility of the gel material that gives rise to stress concentration at the lateral edges of the disk joining the two blocks and consequent propagation of the crack; the difference in stress intensity that occurs along the crack front amplifies any perturbation.

ACKNOWLEDGMENTS

A.G. acknowledges financial assistance in the form of Grant No. IMP/2018/000037 from Science and Engineering Research Board, Government of India.

[1] A. Ghatak, M. K. Chaudhury, V. Shenoy, and A. Sharma, Phys. Rev. Lett. **85**, 4329 (2000).
[2] W. Mönch and S. Herminghaus, Europhys. Lett. **53**, 525 (2001).
[3] V. Shenoy and A. Sharma, Phys. Rev. Lett. **86**, 119 (2001).
[4] A. Ghatak and M. K. Chaudhury, Langmuir **19**, 2621 (2003).
[5] M. K. Chaudhury, A. Chakrabarti, and A. Ghatak, Eur. Phys. J. E **38**, 82 (2015).
[6] A. Gent and P. Lindley, Proc. R. Soc. London, Ser. A **249**, 195 (1959).
[7] A. Cristiano, A. Marcellan, R. Long, C. Y. Hui, J. Stolk, and C. Creton, J. Poly. Sci.: Part B: Poly. Phys. **48**, 1409 (2010).
[8] K. Shull, C. Flanigan, and A. Crosby, Phys. Rev. Lett. **84**, 3057 (2000).
[9] J. Sarkar, V. Shenoy, and A. Sharma, Phys. Rev. E **67**, 031607 (2003).
[10] A. Ghatak, Phys. Rev. E **73**, 041601 (2006).
[11] T.Vilmin, F. Ziebertand, and E. Raphael, Langmuir **26**, 3257 (2010).
[12] M. Gonuguntla, A. Sharma, J. Sarkar, S.A. Subramanian, M. Ghosh, and V. Shenoy, Phys. Rev. Lett. **97**, 018303 (2006).
[13] J. Y. Chung, K. H. Kim, M. K. Chaudhury, J. Sarkar, and A. Sharma, Eur. Phys. J. E **20**, 47 (2006).
[14] A. Ghatak and M. K. Chaudhury, J. Adhes. **83**, 679 (2007).
[15] M. Adda-Bedia and L. Mahadevan, Proc. R. Soc. London, Ser. A **462**, 3233 (2006).
[16] B. Saintyves, O. Dauchot, and E. Bouchaud, Phys. Rev. Lett. **111**, 047801 (2013).
[17] J. S. Biggins, B. Saintyves, Z. Wei, E. Bouchaud, and L. Mahadevan, Proc. Natl. Acad. Sci. USA **110**, 12545 (2013).

[18] C.-Y. Lai, Z. Zheng, E. Dressaire, J. S. Wexler, and H. A. Stone, Proc. R. Soc. A **471**, 20150255 (2015).
[19] P. G. Saffman and G. I. Taylor, Proc. R. Soc. London, Ser. A **245**, 312 (1958).
[20] K. K. Kundan and A. Ghatak, Soft Matter **14**, 1365 (2018).
[21] See Supplemental Material at http://link.aps.org/supplemental/10.1103/PhysRevE.102.013002 for a representative movie of the occurrence and evolution of the instability.
[22] E. Lemaire, P. Levitz, G. Daccord, and H. Van Damme, Phys. Rev. Lett. **67**, 2009 (1991).
[23] H. Van Damme, C. Laroche, and L. Gatineau, Rev. Phys. Appl. (Paris) **22**, 241 (1987).
[24] H. Van Damme, C. Laroche, L. Gatineau, and P. Levitz, J. Phys. (Paris) **48**, 1121 (1987).
[25] B.-m. Z. Newby, M. K. Chaudhury, and H. R. Brown, Science **269**, 1407 (1995).
[26] H. E. Huppert, Nature (London) **300**, 427 (1982).
[27] J. M. Jerrett and J. R. de Bruyn, Phys. Fluid A: Fluid Dyn. **4**, 234 (1992).
[28] Z. N. Silvi and E. B. Dussan V, Phys. Fluid **28**, 5 (1985).
[29] F. Melo, J. F. Joanny, and S. Fauve, Phys. Rev. Lett. **63**, 1958 (1989).
[30] N. Fraysse and G. M. Homsy, Phys. Fluid **6**, 1491 (1994).
[31] A. M. Cazabat, F. Heslot, S. M. Troian, and P. Carles, Nature (London) **346**, 824 (1990).
[32] J. B. Brzoska, F. Brochard-Wyart, and F. Rondelez, Europhys. Lett. **19**, 97 (1992).
[33] C. Spandagos, T. B. Goudoulas, P. F. Luckham, and O. K. Matar, Langmuir **28**, 7197 (2012).
[34] C. Spandagos, T. B. Goudoulas, P. F. Luckham, and O. K. Matar, Langmuir **28**, 8017 (2012).
[35] J. B. Bostwick and K. E. Daniels, Phys. Rev. E **88**, 042410 (2013).
[36] K. L. Johnson, *Contact Mechanics* (Cambridge University Press, Cambridge, UK, 1985).
[37] T. Takigawa, Y. Morino, K. Urayama, and T. Masuda, Polym. Gels Netw. **4**, 1 (1996).
[38] G. Carbone and B. N. J. Persson, Eur. Phys. J. E **17**, 261 (2005).
[39] B. N. J. Persson and E. A. Brener, Phys. Rev. E **71**, 036123 (2005).
[40] C. Creton and M. Ciccotti, Rep. Prog. Phys. **79**, 046601 (2016).
[41] D. S. Dugdale, J. Mech. Phys. Solids **8**, 100 (1960).
[42] For fracture of a soft material, velocity of crack propagation is related to strain energy release rate as [43], $\ln(V) \sim G^{1/2}$.
[43] A. Ghatak, K. Vorvolakos, H. She, D. L. Malotky, and M. K. Chaudhury, J. Phys. Chem. B **104**, 4018 (2000).
[44] T. L. Anderson, *Fracture Mechanics (Fundamentals and Applications)* (Taylor & Francis, London, 2005).
[45] A. Chakrabarti and M. K. Chaudhury, Langmuir **29**, 6926 (2013).